Degradation of zirconia in moisture

Xueqiang Cao [a,*], Robert Vassen [b], Jinshuang Wang [a], Binglin Zou [c], Shibao Li [d], Yu Hui [c],

Jieyan Yuan [a], Wenjia Song [e], Qin Cao [a], Jianing Jiang [a], Longhui Deng [a], Shujuan Dong [a]

[a] *State Key Laboratory of Silicate Materials for Architectures (Wuhan University of Technology, WUT), Wuhan 430070, China.*

[b] *IEK-1, Forschungszentrum Juelich GmbH, D-52425, Deutschland.*

[c] *State Key Laboratory of Rare Earth Resources Utilization, Changchun Institute of Applied Chemistry (CIAC), Chinese Academy of Sciences, Changchun 130022, China.*

[d] *Department of Dental Materials, Fourth Military Medical University, China. Xi'an 710032, China.*

[e] *Department of Earth and Environmental Sciences, Ludwig-Maximilians-Universitaet (LMU) Munich, Theresienstrasse 41/III, 80333 Muenich, Deutschland.*

*Corresponding author. *E-mail address*: xcao@whut.edu.cn.

Abstract

Zirconia especially stabilized by Y_2O_3 (YSZ) is an important and popularly used material. We have observed the degradation of YSZ in moisture, and have also revealed the degradation mechanism which could be related to the following three chemical processes: (1) reaction of water with the residual Y_2O_3 which is not incorporated into the crystal lattice of ZrO_2; (2) corrosion of YSZ by water; (3) depletion of Y^{3+} from the crystal lattice by water molecule due to oxygen vacancies. A core/shell structure of ZrO_2/Y_2O_3 in YSZ crystalline grains has been proved. Calcination of YSZ above 1100°C can prevent the degradation.

Keywords: Zirconia; Degradation; Moisture; Residual yttria; Core/shell structure.

1. Introduction

Zirconia is one of the most important materials due to its high melting point, high strength, high fracture toughness, high hardness, large thermal expansion coefficient, low thermal conductivity, ionic conductivity, chemical resistance and lack of toxicity, and it was even regarded as "ceramic steel" [1]. Zirconia is the base of modern ceramic materials that find applications in numerous fields, including thermal barrier coatings (TBCs) [2], biomedical ceramics [3], solid electrolytes [4], catalysis [5], membranes [6], gas sensors [7] and wear materials [8]. These properties could be even largely improved when it is in nano-state due to the superior sintering behavior [9,10] and superplasticity [11]. Among all these applications, the most important are TBCs for gas turbines and biomedical materials for hip implants and dental restorations.

TBCs find an increasing number of applications to protect high-temperature metallic components due to the goal to achieve increased thermal efficiency [12]. YSZ coatings are deposited on transition pieces, combustion lines, vanes, blades and other hot-path components of gas turbines either to increase the inlet temperature with a consequent improvement of thermal efficiency or to reduce the requirement of cooling air. Since 1990s, the nanostructured YSZ (n-YSZ) coatings deposited by atmospheric plasma spraying (APS) have attracted a lot of research interest because of some superior properties in comparison with the conventional YSZ coatings [13-16]. The porous structure of n-YSZ coatings makes coatings more tolerant against stress, as a result, the thermal shock resistance of n-YSZ coatings was improved [17-23]. n-YSZ coatings also have low thermal conductivity [21,23]. However, there are a few cases about the degradation or even pulverization of n-YSZ coatings for aero and space engines whose coatings have been stored in natural environment less than 3 years before engine running, but the mechanism is not clear so far.

Sato et al [24] reported for the first time that YSZ suffered the low temperature degradation

(LTD) in humid air or water, the chemisorption of H_2O to form OH^- ions at the surface resulted in the loss of strain energy which led to the transformation. The formation of $Y(OH)_3$ was observed at the YSZ surface [25]. Yoshimura et al [26] observed that the degradation was greatly accelerated by high-temperature-high-pressure H_2O, and the degradation could be prevented by increasing dopants or reducing grain sizes [27]. Based on the O1s XPS spectrum of YSZ specimen which was continuously annealed in boiling water for 40 h, it was proved by Guo [28] that the degradation was assumed to accomplish by the annihilation of oxygen vacancies in the ZrO_2 lattice, while the degradation was supposed to propagate along the grain boundaries. Water molecules can be incorporated into the ZrO_2 lattice by filling oxygen vacancies, which leads to the formation of proton defects, the relatively fast diffusion of proton defects most probably controls the degradation process [29]. Chevalier et al [30] summarized the phase transformation mechanism of zirconia, and proposed that LTD in moisture was a kinetic phenomenon in which polycrystalline tetragonal material slowly transformed to monoclinic zirconia over a rather narrow but important temperature range, typically room temperature to around 400°C, depending on the stabilizer, its concentration, and the grain size of the ceramic. It was suggested that LTD was induced by the indiffusion of a moisture species such as –OH, and stress also played important role in the transformation. Zhang's work [31] proves that LTD is driven by the indiffusion of moisture species through oxygen vacancies, and a high dopant content results in a high aging-resistance which follows the trend of $La^{3+} > Nd^{3+} > Al^{3+} > Sc^{3+}$.

In the 1990s, YSZ was introduced in orthopedics as an alternative to alumina because of its high fracture toughness [32,33]. It was firstly reported in 1997 that the standard steam sterilization procedure (134°C, 0.2 MPa) led to surface roughening of femoral head implants of YSZ, and in 2001, all products were recalled owing to fracture risk. The artificial teeth made of n-YSZ went into clinical application about twenty years ago, and some cases of premature

failure in vivo situation have been observed. Even though the degradation phenomenon of YSZ biomedical implants has already been observed, the mechanism is still not clear [33-35]. Nowadays, many applications of zirconia are based on n-YSZ. In order to obtain a density as high as possible, n-YSZ powder or suspension must be used, such as artificial teeth as discussed above, electrolytes of solid oxide fuel cell, electronic membranes, catalyst supports and so on. On the other hand, a lot of the newly developed preparation methods of thin films are related to nano grains or clusters, such as suspension plasma spraying (SPS) [36], solution precursor plasma spraying (SPPS) [37,38], plasma spraying-physical vapor deposition (PS-PVD) [39,40], electron beam-physical vapor deposition (EB-PVD) [41] and so on.

During the study of zirconia materials, we have collected hundreds of samples in the form of coatings, powders, green bodies and teeth from different companies. It is observed that the degradation of YSZ materials in moisture is a widespread phenomenon, especially in the form of n-YSZ. For n-YSZ materials, not only oxygen vacancy, but also residual Y_2O_3 and corrosion by water play important roles. In this paper, the degradation mechanism is clarified and its controlling method is proposed.

2. Experimental

2.1. Materials

n-YSZ powder of P-18 (Santong China) was used as an example for the study of degradation mechanism. Its coatings were deposited on graphite substrates by atmospheric plasma spraying (APS) with a plasma gun Type F4 (Multicoat, Sulzer Metco, Switzerland). Several pieces of artificial teeth were obtained by machining of n-YSZ green body (Wieland, Deutschland), followed by sintering at 1450°C for 2 h. Other n-YSZ powders were obtained from different companies and directly used without any other treatment, mainly including: Zirconia TZ-3Y and Zirconia Zpex® (Tosoh, Japan), YSZ Nanopowder (Sigma-Aldrich, Deutschland),

YSZ198U and NanoX S4007 (Inframat, USA), 205 NS and Metco 6700 (Sulzer Metco, Switzerland).

2.2. Quantitative analysis of residual Y_2O_3 in YSZ

Y_2O_3 is the mostly used structural stabilizer of ZrO_2 in which the lattice position of Zr^{4+} is partially substituted by Y^{3+}. YSZ itself is a very stable material against normal acids such as HCl, HNO_3 and H_2SO_4. During the synthesis of YSZ, if the reaction of Y_2O_3 with ZrO_2 is not complete, the residual Y_2O_3 would exist as impurity at grain boundaries of YSZ. Y_2O_3 is a basic oxide and could be very easily dissolved by diluted HCl, the dissolved Y_2O_3 is then quantitatively analyzed by inductively coupled plasma-optical emission spectrometry (ICP-OES, Thermo iCAP 6000). The experimental procedure is simply described as follows: YSZ material is crushed and milled into fine powder with grain size smaller than 20 μm; a few grams of fine powder (powder weight W_0) are soaked in 20 ml 50 vol% HCl solution at 90°C for 3 h followed by evaporation until drying; 10 ml pure water is added into the powder and sonicated for 15 min (solution weight W_1), the solution is centrifugated (rotation speed above 9,000 rpm) for three times to extract the solution from the powder, concentration of Y^{3+} in the solution (X) is analyzed by ICP-OES. The weight percentage (W) of Y_2O_3 in YSZ is then calculated with Eq.1:

$$W = (\frac{X \cdot W_1}{10,000} \times \frac{88.91 + 16 \times 1.5}{88.91}) \div W_0 \qquad (1)$$

where 88.91 and 16 are atomic weights of Y and O, respectively. The systematic error of this analysis method is -(4%~12%), and the standard deviation is ±5%. The solubility of ZrO_2 in HCl solution is less than 1 ppm. Contents of the residual Y_2O_3 in YSZ samples obtained from different companies are listed in Table 1 for comparison.

2.3. Simulation of YSZ degradation in moisture

In order to accelerate the reaction of YSZ with water in moisture, hydrothermal treatment with Teflon autoclave was applied, and the procedure was following: 65 vol% of an autoclave

5

was added with the deionized water; YSZ sample was fixed at the top part of the autoclave with Teflon sieve, moisture in the autoclave could freely surround the sample; the autoclave was warmed at 150°C for 3 h up to 40 days as needed, the vapor pressure inside was 0.6 MPa; the hydrothermally treated samples were dried at 110°C for 1 h.

2.4. Phase stability analysis

X-ray diffraction (XRD) was applied to analyze the phase stability of YSZ samples. For the analysis of phase transformation and crystalline grain size calculation, XRD was carried out on Rigaku D/max-2500 PC (power 18 kW, scanning rate 1°·min^{-1}, λ=0.15406 nm), and the 2θ value was calibrated by the addition of a small amount of high purity graphite powder (Tianjin Fine Chemicals, China) into the sample. In order to get the more detailed information about phase change of YSZ samples after hydrothermal treatment, XRD was also carried out with beamline 14BL at Shanghai Synchrotron Facility equipped with a Huber diffractometer (18 keV, scanning rate 1.2°·min^{-1}, λ=0.071 nm).

The mean crystalline grain size (D) was calculated using Scherrer′s equation [42]:

$$D = \frac{\lambda K}{\beta cos\theta} \quad (2)$$

where λ is the X-ray wavelength, θ the diffraction angle, K a constant (0.89) and β the corrected full-width half maximum (FWHM). YSZ has three phases, i.e. monoclinic (M), tetragonal (T) and cubic (C). The as-deposited coatings by APS or EB-PVD keep a non-transformable tetragonal structure (T′). M-phase content was calculated with the following equations in which m_M, m_C and $m_{T'}$ are contents of M, C and T′-phases in percentage, respectively [43]:

$$\frac{m_M}{m_{C,T'}} = 0.82\frac{I_M(11-1)+I_M(111)}{I_{C,T'}(111)} \quad (3)$$

$$\frac{m_C}{m_{T'}} = 0.88\frac{I_C(400)}{I_{T'}(400)+I_{T'}(004)} \quad (4)$$

$$m_M = 100 - (m_C + m_{T'}) \quad (5)$$

2.5. Other characterization methods

The morphology of samples was observed by field emission-scanning electron microscopy (FE-SEM, FEI/Philips XL-30), high resolution transmission electron microscopy (HRTEM, Talos F200S) and spherical aberration corrected transmission electron microscope (ACTEM, Titan Cubed Themis G2 300). Geometric phase analysis (GPA) of ACTEM was employed to obtain the dislocation strain field of n-YSZ crystalline grain. Y-distribution in crystalline grain of n-YSZ powder was carried out with X-ray photoelectron spectroscopy (XPS, ESCALAB 250, Thermo Electron Corporation). n-YSZ powder was compacted into small samples with a diameter of 10 mm. In order to analyze the Y-distribution in the depth direction of YSZ crystalline grains, the sample surface was eroded by Ar^+ ions (2 kV, 1.2 μA) step by step for 5~1280 s.

The thermal shock life of a coating was measured in the following way: (1) n-YSZ powder (P-18) was calcined at different temperatures between 600°C and 1200°C for 3 h; (2) the calcined powder was deposited on Ni-based superalloy substrates (25 mm×45 mm×3 mm) with NiCoCrAlY as bond coat by APS with a coating thickness of 300 μm; (3) the coating was heated at 1100°C for 5 min and then suddenly quenched into water. This procedure was repeated until 10% of the coating was lost, and the cycling number was regarded as the thermal shock life of the coating. The life time of a coating deposited with each calcined powder was the averaged value of three samples.

One piece of coating deposited by APS with n-YSZ powder (P-18) has been stored in natural environment, i.e. outdoors in a box which is open to air but without exposure to rain in Wuhan China since April 21 of 2016. The phase stability analysis of this sample by XRD is carried out every 3 months.

3. Results and discussion

3.1. Degradation phenomena of YSZ materials

A turbine vane with n-YSZ coatings, an artificial tooth and knife of n-YSZ were hydrothermally treated, and their morphologies are compared in Fig. 1. After hydrothermal treatment as shown in Fig. 1(c,d), coatings on the vane were seriously pulverized and lost into water, and the metallic substrate could be observed obviously. The suspension in the autoclave was dried at 110ºC, and the residual powder which was lost from the vane was collected for other characterization.

The YSZ tooth was completely destroyed into powder as shown in Fig. 1f. Before hydrothermal treatment, the YSZ tooth had a Vicker's hardness of 12.72±0.03 GPa which was nearly four times as high as that of steel. A small piece of the pulverized tooth was used for SEM observation, and results are shown in Fig. 1g. The tooth was pulverized mainly by intergranular cracking, the bonding among grains was very loose. Under a higher magnification, transgranular cracking could also be clearly observed as shown in Fig. 1h. The hydrothermal treatment also leads to the pulverization of YSZ cutting tool as shown in Fig. 1(i,j).

The phase stability of n-YSZ coating stored in natural environment for 4 years is shown in Fig. 2. This sample has not been pulverized but phase change is obvious. M-phase content (m_M, mole%) in the coating is linearly proportional to storing time (t, months):

$$m_M = 1.6 + 0.128t \quad (6)$$

On the other hand, it is clearly indicated in Fig. 2 that the phase change in Spring to Autumn is fast due to both the high atmospheric temperature and humidity. In Winter, the phase change is slow or even stops due to the cold and dry weather.

3.2. Degradation mechanisms

3.2.1. Residual Y₂O₃

(1) Observation of residual Y_2O_3 in YSZ

All rare earth oxides are chemically basic, easily to absorb moisture and carbon dioxide in

air with formations of $Y(OH)_3$ and $Y_2(CO_3)_3$, respectively. In a solid material, impurities are often concentrated at grain boundaries of the main composition. Both reactions of Y_2O_3 with moisture and carbon dioxide are processes with large volume expansion. Therefore, if YSZ material contains a lot of residual Y_2O_3 and is stored in humid air for a long time, intergranular cracking of the material will occur.

In order to observe the existence of residual Y_2O_3 in YSZ, 10 g of the powder P-18 were soaked in the diluted HCl solution at $90^\circ C$ for 3 h. The sample was vaporized at $90^\circ C$ until dry powder was obtained, then 10 ml water was added into the powder followed by centrifugation to extract the solution from the powder. The residual Y_2O_3 in the powder was 0.327% as analyzed by ICP-OES of the clear solution. NaOH solution was added into the above clear solution, leading to the formation of milky white precipitate $Y(OH)_3 \cdot nH_2O$ as shown in Fig. 3a(1) (neutral red was added for clear observation). P-18 was calcined at $1200^\circ C$ for 3 h, the content of residual Y_2O_3 was largely reduced to 0.00185% (Fig. 3a(2)).

High content of residual Y_2O_3 was very dangerous to the stability of YSZ material in moisture. We have analyzed residual Y_2O_3 in hundreds of YSZ samples obtained from different companies, and some results are listed in Table 1 in which crystalline grain sizes of the powders are compared, too. A smaller crystalline grain size corresponds to a higher content of residual Y_2O_3. The powder from Sigma Aldrich has a superfine crystalline grain size of 7 nm, its residual Y_2O_3 content is as high as 1.910%. P-18 is a frequently used powder but unstable in moisture, it has a crystalline grain size of 20 nm and high residual Y_2O_3 content (0.327%). The green body for teeth from Wieland contains 0.122% residual Y_2O_3, and teeth based on this material are unstable in moisture which was shown in Fig. 1. The powder from Xi An has a crystalline grain size of 83 nm, its residual Y_2O_3 content is very low (0.00287%), and its coating is stable in moisture.

During APS, most particles in the powder are molten, but more than 30% semi- or unmelted

particles must be preserved to keep the nano property of materials. The content of residual Y_2O_3 in APS coatings of P-18 was 0.0215%.

YSZ targets for EB-PVD were synthesized by solid state reaction of ZrO_2 with Y_2O_3 at 1500°C for several hours. The content of residual Y_2O_3 in targets was 0.0474%, but largely increased to 0.380% in EB-PVD coatings due to the decomposition of YSZ by electron beam evaporation. If EB-PVD coatings were immediately used at high temperature, then the residual Y_2O_3 would be re-dissolved into the crystal lattice of ZrO_2, and its content was reduced to 0.170% (1000°C for 1 h) and 0.114% (1100°C for 1 h), respectively; if coatings were hydrothermally treated for 40 days, the value was increased to 0.415%, indicating more Y_2O_3 had been depleted from the crystal lattice of ZrO_2.

Metco 6700 from Sulzer Metco is a mixture of Y_2O_3 and ZrO_2 which is specially designed for PS-PVD. Its PS-PVD coating had 0.222% of residual Y_2O_3 and nearly no M-phase was observed; after hydrothermal treatment for 10 days, the residual Y_2O_3 content was increased to 0.253%, and 5.2% M-phase was formed.

(2) Why residual Y_2O_3 exists?

For commercial YSZ powders, there are basically two ways to synthesize, i.e. solid state and solution methods. In the former way, mixture of Y_2O_3 and ZrO_2 is heated directly above 1500°C for a few hours, Y^{3+} ions diffuse into the crystal lattice of ZrO_2, and the higher is the temperature, the more complete is the reaction, in other words, less residual Y_2O_3 is left.

A lot of commercial n-YSZ powders are obtained by solution method with a much lower calcination temperature normally below 900°C (mostly 500°C~700°C), including co-precipitation, Sol-Gel, hydrothermal synthesis, emulsion synthesis, and so on [44]. Co-precipitation is usually used for large quantity production, and its procedure could be simply described as follows [44,45]: (1) ammonia solution is added slowly into the mixture solution of YCl_3 and $ZrOCl_2 \cdot 8H_2O$, leading to the formation of hydroxide mixture of $Y(OH)_3$ and

ZrO(OH)$_2$; (2) hydroxide mixture is heated at a comparatively low temperature to form nano powders. In order to make the mixing of hydroxides more uniform, the hydroxide mixture could be transferred into autoclave for hydrothermal treatment followed by heating to form nano powders. However, co-precipitation of Y(OH)$_3$ and ZrO(OH)$_2$ actually does not occur due to the large difference between the solubility product constants (K_{sp}) of these two precipitates: K_{sp}[ZrO(OH)$_2$]=6.3×10^{-49}, K_{sp}[Y(OH)$_3$]=8×10^{-23}. If molar concentrations of Y^{3+} and ZrO^{2+} in the mixture solution of YCl$_3$ and ZrOCl$_2$ are 0.1 M and 1 M, respectively, the lowest concentrations of OH$^-$ to form Y(OH)$_3$ and ZrO(OH)$_2$ are 8.9×10^{-7} M and 7.9×10^{-25} M, respectively. Obviously, the latter is nearly 18 orders of magnitude lower than the former, in other words, ZrO(OH)$_2$ is much more preferentially to precipitate than Y(OH)$_3$. Therefore, in the hydroxide mixture, the so-called "co-precipitate" particle must be the core of ZrO(OH)$_2$ (Zr-core) with a shell of Y(OH)$_3$ (Y-shell). In the subsequent calcination, Y^{3+} from Y-shell diffuses into Zr-core with the formation of YSZ. If the calcination temperature is below 900°C, Y^{3+} diffusion occurs mainly in the top thin layer of Zr-core (surface diffusion); only above 900°C, Y^{3+} diffuses deeply into Zr-core (bulk diffusion). During the synthesis of n-YSZ powder, in order to keep a crystalline grain size as small as possible, the calcination temperature is normally below 900°C, unavoidably resulting in the formation of residual Y$_2$O$_3$.

Fig. 3b strongly proves the existence of Zr-core with Y-shell in an YSZ crystalline grain. n-YSZ grains with different treatments are bombarded with Ar+ ions for 0~1280 s to remove Y-shells step by step, Y-distributions in the depth direction are then measured by XPS. Curve 1 is for P-18 powder without any treatment. Y-distribution is nearly constant when the bombarding time is shorter than 80 s. Above 160 s, Y-distribution continuously decreases until 640 s, and the Y-distribution still keeps a low and constant value even the bombarding time is as long as 1280 s. This measurement indicates that Y concentrates in the grain surface layer to form Y-shell, and a bombarding time of 640 s is necessary to destroy Y-shell.

If n-YSZ is calcined at 1200°C for 3 h, Y-distribution is nearly a constant value as shown in Curve 2, indicating that Y^{3+} diffusion from Y-shell into Zr-core is completed at 1200°C and Y-shell nearly disappears.

If n-YSZ is hydrothermally treated, Y^{3+} would diffuses out of Zr-core into Y-shell, and this proposal is proved by Curve 3. n-YSZ was hydrothermally treated for 10 days and then washed thoroughly with HCl solution to remove Y-shell, it is obvious that Y-distribution is decreased from the inside to the outside. The loss of structural stabilizer Y_2O_3 is the main reason for phase transformation T→M. The M-phase formation involves a large volume expansion, making both intergranular and transgranular cracks in zirconia materials.

The core/shell structure of Zr/Y could be observed by HRTEM as shown in Fig. 4. HRTEM and XRD of n-YSZ powder calcined at 500°C were shown in Fig. 4(a,b). By accurate calculation of d-spacings, we can define crystal structures of some crystalline grains, including T, M-phases of YSZ and Y_2O_3 as shown in Fig. 4a. The powder is seriouly agglomerated, and only some grains are monodispersed such as Fig. 4(c,e). Due to the low calcination temperature, the reaction between $Y(OH)_3$ and $ZrO(OH)_2$ is not complete, the grain size is about 2-20 nm, and all main peaks of T-phase in XRD are obviously seperated into two peaks. The d-spacing difference between two peaks of T(101) is 0.0019 nm. HRTEM of a crystalline grain with plane T(101) is shown in Fig. 4c, in which a Y_2O_3 grain is observed. Along the crystal plane, d-spacings of seven positions are compared in Fig. 4d, and each d-spacing is an average value of 10~20 planes. It is obvious that a core/shell structure really exists in the grain. Y^{3+} (0.091 nm) has a larger radius than Zr^{4+} (0.074 nm), resulting in an increase of d-spacing when Y^{3+} diffusses into the crystal lattice of T-ZrO_2. The T(101) d-spacing difference between the surface and center of the grain is about 0.0032 nm with a median value 0.0016 nm, very similar to the XRD result. HRTEM of a crystalline grain with plane M(-111) and the d-spacing distribution are shown in Fig. 4(e,f), respectively. The surface has a smaller d-spacing than the center because

the phase transformation M→T is a volume shrinkage process. Based on Fig. 4(c-f), the thickness of Y-shell is estimated to be 2~3 nm.

Geometric phase analysis (GPA) was employed to obtain the dislocation strain field as shown in Fig. 5. The stress distribution also forms a core/shell structure which is similar to the observation in Fig. 4. On the other hand, the stress location is at the place close to Zr^{4+}/Y^{3+}atoms, which is the location where most possibly with oxygen vacancy. As mentioned above, in the surface layer of n-YSZ crystalline grain, Y^{3+} concentration is higher than the inside, forming a Zr^{4+}-core/Y^{3+}-shell structure and resulting in a shell with high concentration of oxygen vacancy.

Effects of both heat and hydrothermal treatments on the core/shell structure are simply described with Fig. 6. Effect of hydrothermal treatment leads to the out-diffusion of Y^{3+} ions from the core to shell, and the heat treatment at high temperatures results in the in-diffusion of Y^{3+} ions from the shell into core.

(3) Controlling residual Y₂O₃

P-18 powder was heated at different temperatures for 3 h, both residual Y_2O_3 and M-phase were quantitatively analyzed, and results are shown in Fig. 7a. The content of residual Y_2O_3 is nearly constant below 800℃, and it is largely reduced above 900℃ until a low constant value above 1100℃, implying that Y^{3+} diffusion from Y-shell into Zr-core starts at 900℃ and leads to nearly a homogenous distribution at 1100℃, and this conclusion coincides with Fig. 3b. The effect of heating temperature on residual Y_2O_3 could be exactly simulated with the following equation:

$$[Y_2O_3] = -0.008 + \frac{0.332}{1+\exp(\frac{T-961.1}{55.7})} \quad (7)$$

where $[Y_2O_3]$ is residual Y_2O_3 (wt%) and T (℃) the heating temperature with a duration longer than 1 h. Accordingly, more Y^{3+} from Y-shell diffuses into Zr-core with the increase of heating temperature, resulting in the reduction of M-phase as shown also in Fig. 7a.

The duration of heating time is not always effective to control residual Y_2O_3 and M-phase as

shown in Fig. 7b. At 1000°C, both the content of residual Y_2O_3 and M-phase are simultaneously reduced with the increase of heating duration till 45 min, and then keep nearly constant even though the duration is as long as 2 h, implying that Y^{3+} diffusion from Y-shell into Zr-core at 1000°C is finished within 45 min and time elongation is no longer meaningful. At 800°C, the time duration of 2 h is necessary for Y^{3+} diffusion to reach an equilibrium. On the other hand, the content of residual Y_2O_3 is inversely proportional to the heating time as shown in Curve 1 of Fig. 7b, which could be simulated very well with the following equation:

$$Ln[Y_2O_3]_t = Ln[Y_2O_3]_0 - kt = -5.7378 - 0.7525t \qquad (8)$$

where $[Y_2O_3]_0$ and $[Y_2O_3]_t$ (wt%) are contents of residual Y_2O_3 at heating time=0 and t (h), respectively, k the rate constant. Eq. 8 proves that the diffusion of Y^{3+} ions inside ZrO_2 crystal lattice is the first order reaction which has also been indicated in Eq. 6. During heating, the crystalline grain size (D, nm) of n-YSZ will also increases, and the relation of crystalline grain size [Ln(D)] as a function of heating temperature [1000/(T, K)] is shown in Curve 1 of Fig. 7c. This curve consists of two straight lines with a turn point close to 900°C. The relation between crystalline grain size and heating temperature could be described with the following equation:

$$D_T = D_0 \times e^{(-\frac{E_a}{RT})} \qquad (9)$$

where D_T is the crystalline grain size at temperature T, D_0 the original crystalline grain size before heating, E_a (kJ·mol^{-1}) the active energy for crystalline grain growth, R the ideal gas constant (8.314 J·mol^{-1}·K^{-1}). Ionic diffusions occurs in the surface layer (surface diffusion) below 900°C, and the bulk diffusion occurs above 900°C. With Eq. 9, active energies for both surface and bulk diffusions are obtained: 4.3 kJ.mol^{-1} (<900°C), 28.3 kJ.mol^{-1} (>900°C), and the latter process is obviously much more difficult than the former one.

A lot of authors reported that n-YSZ coatings had longer thermal shock lives than conventional coatings, but some results were opposite. These contradictory results come from different powders with different compositions, crystalline grain sizes and morphologies.

Therefore, results based on different powders are not suitable for comparison. Powder P-18 was heated at different temperatures for 3 h, crystalline grain sizes of these thermally treated powders are largely different, but other properties are little influenced. Thermal shock lives of APS coatings made of such thermally treated powders are compared also in Curve 2 of Fig. 7c. Below 900°C, the crystalline grain size does not increase obviously (23 nm for 900°C); at higher temperature, the crystalline grain size increases largely (30 nm for 1000°C). Below 900°C, thermal shock lives are nearly the same (179±18 cycles); above 900°C, thermal shock lives are suddenly reduced to a low value (85±20 cycles). The life of the coating whose powder is calcined below 900°C is double that whose powder is calcined above 900°C. In other words, only the coating whose powder has a crystalline grain size smaller than 23 nm would have an obviously long thermal shock life.

However, the stability of n-YSZ coatings in moisture is opposite to its thermal shock life. The synthesis of n-YSZ powder always needs a comparatively low temperature normally below 900°C, and its coating has a long thermal shock life, but the content of residual Y_2O_3 would be on a high level, and the risk to be pulverized by moisture is also high.

3.2.2. Corrosion by water

n-YSZ coatings of powder P-18 were hydrothermally treated for 3 h~40 days, and their morphologies are shown in Fig. 8. Fig. 8a shows the typical microstructure of plasma-sprayed coatings, including mainly equiaxed grains and some columnar grains [46]. The equiaxed and columnar grains with large magnifications are shown in Fig. 8(b,e). After hydrothermal treatment for 10 days, n-YSZ coatings were cracked into small pieces, showing a transitional state before pulverization. Before hydrothermal treatment, the equiaxed grains were bonded to each other tightly (Fig. 8a) and have smooth surfaces and sharp edges (Fig. 8(b,c)). Serious intergranular cracking are observed after hydrothermal treatment (Fig. 8d), and more interestingly, edges and surfaces of some grains were seriously corroded (Fig. 8(e,f)), numerous

corrosion pits were formed into the grain surface, and even a transgranular cracking shallowly into a grain was observed.

After being hydrothermally treated at 150°C for 40 days, n-YSZ coatings were nearly dissolved into water with the formation of "TBCs milk" as shown in Fig. 8g. The "TBCs milk" was evaporated, forming a very fine powder, and its morphology was shown in Fig. 8h in which semi- or unmelted particles, equiaxed and columnar grains are more clearly observed. The grains were seriously spheroidized, grain surfaces and edges are corroded (Fig. 8i).

Effects of hydrothermal treatment on crystalline grain size, residual Y_2O_3 and M-phase transformation are shown in Fig. 8(j~l). With the increase of hydrothermal treatment duration, the crystalline grain size decreases until an equilibrium value, and approximately 8 days are necessary to reach such equilibrium (Fig. 8j), strongly proving that YSZ grains are dissolved by water. The corrosion of YSZ grains also leads to Y^{3+} depletion of from YSZ crystal lattice, resulting in the increase of residual Y_2O_3 and M-phase transformation as shown in Fig. 8k, and 8 days are also necessary to reach the equilibrium. With XRD by synchrotron, the phase transformation of YSZ coatings after hydrothermal treatment is clearly observed as shown in Fig. 8l.

3.2.3. Effect of oxygen vacancy

There is no direct and solid evidence to prove that oxygen vacancies really accelerate the degradation of YSZ. However, we have observed some indirect evidences as follows. In the EB-PVD process, the top part of 8YSZ target is fully molten and vaporized by electron beam in vacuum. When the target is cooled, the molten YSZ is solidified and the color changes from white to gray or dark (Fig. 9a) depending on the oxygen loss, i.e. formation of oxygen vacancy. The higher is the oxygen vacancy content, the darker it looks. We found that the dark target is very easy to be pulverized by moisture as shown in Fig. 9b. The thermal gravimetric analysis (TGA) of 8YSZ target in air atmosphere is shown in Fig. 9c, in which the red and black curve

As proved above, Y^{3+} ions are mainly concentrated in the surface layer of n-YSZ grains if calcination temperature is below 900°C. In YSZ, $2Y^{3+}$ substitute for $2Zr^{4+}$, leading to the formation of one oxygen vacancy ($V_O^{..}$, Kroeger-Vink notation) which is electrically positive. Due to Coulomb and elastic attractive forces between Y_{Zr}' and $V_O^{..}$,, the formation of defect associates ($Y_{Zr}'V_O^{..}$) is possible. Therefore, we can suppose the situation of n-YSZ grains whose surfaces are covered by oxygen vacancies and dangling bonds (Fig. 10a). The reaction between H_2O molecules and n-YSZ surfaces is simply described in Fig. 10b. In contact with H_2O, O atoms of H_2O occupies oxygen vacancies, and H atoms of H_2O bond with O atoms of n-YSZ with the formation of hydrogen bond (H-bond). Chemical bonds formed on surfaces of n-YSZ grains are described with the following defect reaction:

$$Y_2O_3 \overset{ZrO_2}{\longleftrightarrow} 2Y_{Zr}' + 3O_O^\times + V_O^{..} \text{ [30]} \qquad (10)$$

$$H_2O + V_O^{..} + O_O^\times = 2(O-H)^{.} \qquad (11)$$
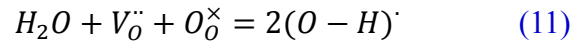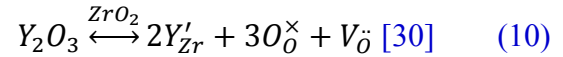
Both Y^{3+} and Zr^{4+} ions combine with OH groups, giving rise to the formation of $Y(OH)_3$ and $ZrO(OH)_2$ and depletion of both Y^{3+} and Zr^{4+} ions from n-YSZ grains (Fig. 10c). This process is described with the following defect reaction:

$$2Y_{Zr}' + V_O^{\bullet\bullet} + 3Zr_{Zr}^\times + 9O_O^\times + 6H_2O = 2Y(OH)_3 + 3ZrO(OH)_2 \qquad (12)$$
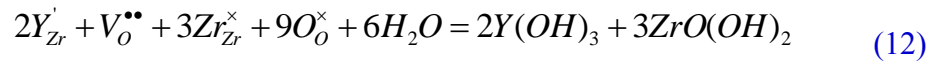
Eq. 12 explains the corrosion process of YSZ grains by water. Accordingly, the loss of Y^{3+} is the key to ignite M-phase transformation, and this is the reason for the formation of transgranular cracking in YSZ grains as shown in Fig. 1h and Fig. 8f. On the other hand, as demonstrated in Fig. 8f, the corrosion of YSZ grains starts at grain corners followed by edges and surfaces, because every atom at corners has the most dangling bonds.

Even though the equiaxed and columnar grains in YSZ coatings have a size much larger than nanometer, they contain a lot of oxygen vacancies which can accelerate the reaction between YSZ grains and H_2O. Studies on YSZ electrolyte prove that both Y'_{Zr} and $V_O^{\cdot\cdot}$ enrich in the grain boundary core when the crystalline grain size is smaller than 41 nm [47], and nano-YSZ electrolyte shows protonic conduction due to the surface reaction between $V_O^{\cdot\cdot}$ and H_2O [48]. On the other hand, $V_O^{\cdot\cdot}$ in YSZ are also formed due to the fast cooling during APS or EB-PVD. The above description could be applied to explain effects of H_2O on YSZ grains, including grain size reduction, depletion of Y^{3+} and M-phase transformation.

Alkali oxides such as MgO and CaO are also structural stabilizers of ZrO_2, MgO and CaO are more basic and water-sensitive than Y_2O_3. The hydrothermal treatment of both MgO-ZrO_2 and CaO-ZrO_2 demonstrated that their degradation problem and depletion of Ca^{2+}/Mg^{2+} were much more serious than those of YSZ, proving that basicity of the stabilizer was also important to the stabilization of zirconia materials in moisture. Another reason for the easier degradation of MSZ and CSZ is the higher concentration of oxygen vacancy than YSZ if Ca^{2+}/Mg^{2+} and Y^{3+} have the same molar concentrations.

Zhang's work [31] indicates that the aging-resistance follows the trend of $La^{3+} > Nd^{3+} >$ $Al^{3+} > Sc^{3+}$, and a high dopant content results in a high aging-resistance. A high dopant content leads to a high oxygen vacancy content and also a high reaction rate of oxygen vacancy with water molecule. On the other hand, a high dopant content also leads to a low transformation from T to M-phase. During the hydrothermal aging process, water moleclue reacts with dopant ion through oxygen vacancy, the outwards diffusion of dopant is related to the ionic size, in other words, a large ion has a slow ionic diffusion, and also slow aging rate.

3.3. Controlling degradation

As discussed above, the degradation of YSZ materials is an integrated result of residual Y_2O_3, corrosion by water and oxygen vacancy, and all these three factors are related to crystalline

grain size. The small size is a result of low-temperature synthesis, and of course the content of residual Y_2O_3 is high. The nanosized grains have high specific surface area, oxygen vacancies are concentrated in the grain surface layer, and grains are also easily to be corroded by water.

The best method to control pulverization is the synthesis temperature of the powder to be above 1100°C. At this temperature, the bulk diffusion of Y^{3+} ions from Y-shell into Zr-core is nearly complete and Y-shell disappears which is very helpful to the stabilization of crystalline grains. The crystalline grain size is normally in the range of 30~40 nm and the content of residual Y_2O_3 is on a low level (0.0076 wt%). APS coatings made of powder P-18 which was calcined at 1100°C for 3 h has much better stability in moisture.

Another method to control pulverization of YSZ coatings is to thermally treat the coating at 1100°C for 3 h. Such post-heat treatment is especially helpful to coatings made by EB-PVD because the as-deposited coatings have high content of residual Y_2O_3 (0.380%). Two positive effects are resulted from such post-heat treatment, including the reduction of residual Y_2O_3 and grain growth of the semi- and unmelted particles (in APS coatings). This method is limited by the application temperature of superalloy substrate.

4. Conclusion

The residual Y_2O_3 in YSZ materials is quantitatively analyzed. There are three factors to influence the stability of YSZ in moisture, including residual Y_2O_3, corrosion by water and oxygen vacancy. The smaller is the crystalline grain size, the more dangerous is the material to be corroded. During the synthesis of YSZ powder by solution method, Y-shell is formed on top of Zr-core if calcination temperature is below 900°C, the bulk diffusion of Y^{3+} is complete above 1100°C which is very helpful to the stability of YSZ materials. A high content of residual Y_2O_3 usually corresponds to a small crystalline grain size of YSZ and the existence of Zr-core/Y-shell structure, both contents of Y^{3+} and oxygen vacancy in Y-shell are high, and the

corrosion of YSZ by water is fast. Post-treatment of the YSZ coatings in air atmosphere above 1100°C could largely reduce the content of residual Y_2O_3 and oxygen vacancies in Y-shell, giving rise to the reduction of degradation risk.

References

[1] R. C. Garvie, R. H. Hannink, R. T. Pascoe, Ceramic steel? *Nature* 258 (1975) 703-704.

[2] N. Padture, M. Gell, E. Jordan, Thermal barrier coatings for gas turbine engine applications, *Science* 296 (2002) 280-284.

[3] J. Chevalier, L. Gremillard, Anil V. Virkar, David R. Clarke, The tetragonal-monoclinic transformation in zirconia: lessons learned and future trends, *J. Am. Ceram. Soc.* 92 [9] (2009) 1901-1920.

[4] N. Q. Minh, Ceramic fuel-cells, *J. Am. Ceram. Soc.* 76 [3] (1993) 563-588.

[5] T. Yamaguchi, Application of ZrO_2 as a catalyst and a catalyst support, *Catal. Today* 20 [2] (1994) 199-218.

[6] R. S. Pavlik Jr., L. C. Klein, R. A. McCauley, Zirconia gels in concentrated NaOH, *J. Am. Ceram. Soc.* 78 [1] (1995) 221-224.

[7] E. Haefele, K. Kaltenmaier, U. Schoenauer, Application of the ZrO_2 sensor in determination of pollutant gases, *Sensor. Actuat. B-Chem.* 4 [3-4] (1991) 525-527.

[8] E. Tocha, H. Schoenherr, G. J. Vancso, N. Siebelt, Influence of grain size and humidity on the nanotribological properties of wear-resistance nanostructured ZrO_2 coatings: an atomic force microscopy study, *J. Am. Ceram. Soc.* 88 [9] (2005) 2498-2503.

[9] G. Skandan, Processing of nanostructured zirconia ceramics, *Nanostruct. Mater.* 5 [2] (1995) 111-126.

[10] V. V. Srdic, M. Winterer, H. Hahn, Sintering behavior of nanocrystalline zirconia prepared by chemical vapor synthesis, *J. Am. Ceram. Soc.* 83 [4] (2000) 729-736.

[11] G. Chen, K. Zhang, Superplastic extrusion of Al_2O_3-YTZ nanocomposite and its deformation mechanism, *Mater. Sci. Forum* 475-479 (2005) 2973-2976.

[12] John H. Perepezko, The hotter the Engine, the better, *Science* 326 (2009) 1068-1069.

[13] R. S. Lima, B. R. Marple, Thermal spray coatings engineered from nanostructured ceramic agglomerated powders for structural, thermal barrier and biomedical applications: a review, *J. Therm. Spray Technol.* 16 [1] (2007) 40-63.

[14] M. Gell, Application opportunities for nanostructured materials and coatings, *Mater. Sci. Eng. A* 204 (1995) 246-251.

[15] M. Gell, The potential for nanostructured materials in gas turbine engines, *Nanostruct. Mater.* 6 (1995) 997-1000.

[16] C. C. Berndt, P. Michlik, O. Racek, Proceedings of the international thermal spray

conference (ITSC 2004), Osaka, Japan, 2004, p. 1110.

[17] B. Liang, C. Ding, Thermal shock resistances of nanostructured and conventional zirconia coatings deposited by atmospheric plasma spraying, *Surf. Coat. Technol.* 197 (2005) 185-192.

[18] H. Jamalin, R. Mozafarinia, R. S. Razavi, R. Ahmadi-Pidani, Comparison of thermal shock resistances of plasma-sprayed nanostructured and conventional yttria stabilized zirconia thermal barrier coatings, *Ceram. Inter.* 38 (2012) 6705-6712.

[19] C. G. Zhou, N. Wang, H. B. Xu, Comparison of thermal cycling behavior of plasma sprayed nanostructured and traditional thermal barrier coatings, *Mater. Sci. Eng. A* 452-453 (2007) 569-574.

[20] R. S. Lima, B. R. Marple, Nanostructured YSZ thermal barrier coatings engineered to counteract sintering effects, *Mater. Sci. Eng. A* 485 [1-2] (2008) 182-193.

[21] A. Keyvani, M. Saremi, M. Heydarzadeh Sohi, Z. Valefi, A comparison on thermomechanical properties of plasma-sprayed conventional and nanostructured YSZ TBC coatings in thermal cycling, *J. Alloys Comp.* 541 (2012) 488-494.

[22] J. Wu, H. Guo, L. Zhou, L. Wang, S. K. Gong, Microstructure and thermal properties of plasma sprayed thermal barrier coatings from nanostructured YSZ, *J. Therm. Spray Technol.* 19 [6] (2010) 1186-1194.

[23] R. S. Lima, B. R. Marple, Toward highly sintering-resistant nanostructured ZrO_2-7wt%Y_2O_3 coatings for TBC applications by employing differential sintering, *J. Therm. Spray Technol.* 17 [5-6] (2008) 846-852.

[24] T. Sato, M. Shimada, Transformation of yttria-doped tetragonal ZrO_2 polycrystals by annealing in water, *J. Am. Ceram. Soc.* 68 [6] (1985) 356-359.

[25] F. F. Lange, G. L. Dunlop, B. I. Davis, Degradation during aging of transformation-toughened ZrO_2-Y_2O_3 materials at 250ºC, *J. Am. Ceram. Soc.* 69 [3] (1986) 237-240.

[26] M. Yoshimura, T. Noma, K. Kawabata, S. Somiya, The role of H_2O on the degradation

process of Y-TZP, *J. Mater. Soc.y Lett.* 6 [4] (1987) 465-467.

[27] M. Yoshimura, Phase stability of zirconia, *Am. Ceram. Soc. Bull.* 67 [12] (1988) 1950-1955.

[28] X. Guo, Low temperature degradation mechanism of tetragonal zirconia ceramics in water: role of oxygen vacancies, *Solid State Ionics* 112 (1998) 113-116.

[29] X. Guo, Property Degradation of Tetragonal Zirconia Induced by Low-Temperature Defect Reaction with Water Molecules, *Chem. Mater. 16 (*2004) 3988-3994.

[30] J. Chevalier, L. Gremillard, The tetragonal-monoclinic transformation in zirconia: lessons learned and future trends, *J. Am. Ceram. Soc.* 92 [9] (2009) 1901-1920.

[31] F. Zhang, M. Batuk, J. Hadermann, G. Manfredi, A. Marien, K. Vanmeensel, M. Inokoshi, B. V. Meerbeek, I. Naert, J. Vleugels, Effect of cation dopant radius on the hydrothermal stability of tetragonal zirconia: grain boundary segregation and oxygen vacancy annihilation, *Acta Mater.* 106 (2016) 48-58.

[32] B. Cales, Zirconia as a sliding material: histologic, laboratory, and clinical data, *Clin. Orthopaed. Relat. Res.* 379 (2000) 94-112.

[33] I. C. Clarke, M. Manaka, D. D. Green, P. Williams, G. Pezzotti, Y. H. Kim, Current status of zirconia used in total hip implants, *J. Bone Joint Surg.* 85-A (2003) 73-84.

[34] J. Chevalier. What future for zirconia as a biomaterial? *Biomaterials* 27 (2006) 535-543.

[35] J. Chevalier, L. Gremillard, S. Deville, Low-temperature degradation of zirconia and implications for biomedical implants, *Ann. Rev. Mater. Res.* 37 (2007) 1-32.

[36] N. Curry, K. V. Every, T. Snyder, N. Markocsan, Thermal conductivity analysis and lifetime testing of suspension plasma-sprayed thermal barrier coatings, *Coatings* 4 (2014) 630-650.

[37] E. Brinley, K. S. Babu, S. Seal, The solution precursor plasma spray processing of nanomaterials, *JOM* 59 [7] (2007) 54-59.

[38] L. Pawlowski, Suspension and solution thermal spray coatings, *Surf. Coat. Technol.* 203 (2009) 2807-2829.

[39] S. Rezanka, G. Mauer, R. Vaßen, Improved thermal cycling durability of thermal barrier coatings manufactured by PS-PVD, *J. Therm. Spray Technol.* 23 [1-2] (2014) 182-189.

[40] G. Mauer, Plasma characteristics and plasma-feedstock interaction under PS-PVD process conditions, *Plasma Chem. Plasma Proc.* 34 [5] (2014) 1171-1186.

[41] A. Azzopardi, R. Mevrel, B. Saint-Ramond, E. Olson, K. Stiller, Influence of aging on structure and thermal conductivity of Y-PSZ and Y-FSZ EB-PVD coatings, *Surf. Coat. Technol.* 177-178 (2004) 131-139.

[42] H. Y. Jin, N. Wang, L. Xu, S. Hou, Synthesis and conductivity of cerium oxide nanoparticles, *Mater. Lett.* 64 (2010) 1254-56.

[43] Robert A. Miller, James L. Smialek, Ralph G. Garlick, Phase stability in plasma-sprayed, partially stabilized zirconia-yttria, *Adv. Ceram.* 3 (1981) 241-253.

[44] X. Q. Cao, New materials and structures for thermal barrier coatings (in Chinese), Science Press, Beijing China, 2006, Page 76-79.

[45] D. F. Li, K. L. Zeng, X. C. Huang, X. J. Ji, Y. G. Yu, Z. D. Li, X. W. Jie, Synthesis of nano zirconia powders for thermal barrier coatings (in Chinese), Patent CN 101200375A.

[46] R. W. Trice, Y. J. Su, J. R. Mawdsley, K. T. Faber, A. R. De Arellano-Lopez, H. Wang, W. D. Porter, Effect of heat treatment on phase stability, microstructure, and thermal conductivity of plasma-sprayed YSZ, *J. Mater. Sci.* 37 [11] (2002) 2359-2365.

[47] X. Guo, Hydrothermal degradation mechanisms of tetargonal zirconia, *Mater. Sci.* 36 (2001) 3737-3744.

[48] G. Chiodelli, F. Maglia, U. Anselmi-Tamburin, Z. A. Munir, Characterization of low temperature protonic conductivity in bulk nanocrystalline fully stabilized zirconia, *Solid State Ionics* 180 [4-5] (2009) 297-301.

Fig. 1. Photographs and SEM of a turbine vane with n-YSZ coatings before (a,b) and after hydrothermal treatment for 10 days (c,d); YSZ teeth before (e) and after hydrothermal treatment for 22 days (f~h); YSZ cutting tool before (i) and after hydrothermal treatment for 10 days (j).
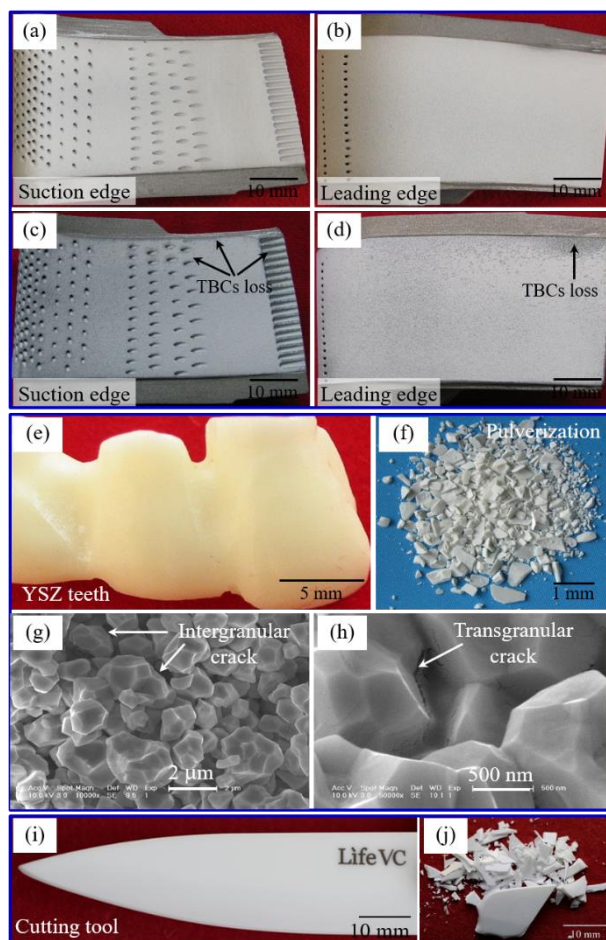
Fig. 2. M-phase content in n-YSZ coatings after being stored in natural environment of Wuhan of China for different periods. XRD was carried out to measure M-phase every 3 months. H and T are the averaged absolute atmospheric humidity and temperature of recent years, respectively.
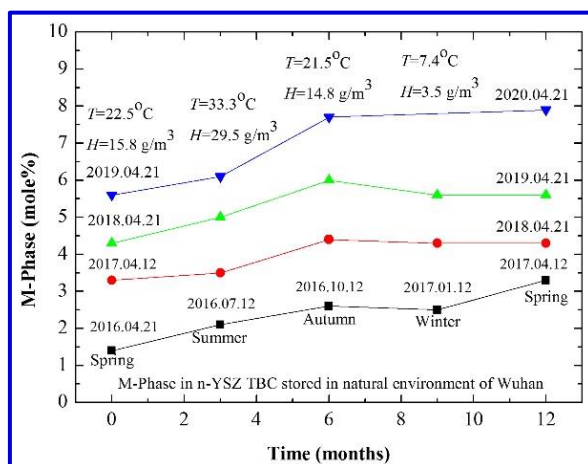
Fig. 3. (a) Precipitates from the original n-YSZ powder (P-18, Bottle 1) and the powder was calcined at 1200°C for 3 h (Bottle 2); (b) Y-contents (Y/(Y+Zr)) in grain surfaces of n-YSZ powders after Ar$^+$ erosion for 5~1280 s by XPS: Curve 1 for the original n-YSZ powder, Curve 2 for the powder calcined at 1200°C for 3 h, Curve 3 for the powder after hydrothermal treatment for 10 days followed by washing with HCl solution.
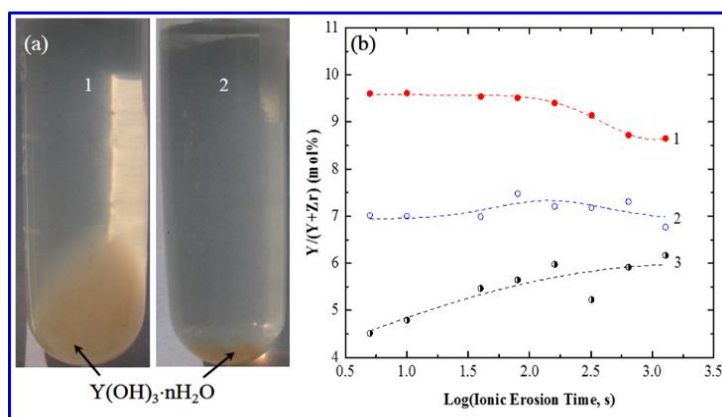
Fig. 4. (a) HRTEM of n-YSZ powder and (b) its XRD; (c) HRTEM of a crystalline grain with T(101) plane and (d) the d-spacing distribution; (e) HRTEM of a crystalline grain with M(-111) plane and (f) the d-spacing distribution.
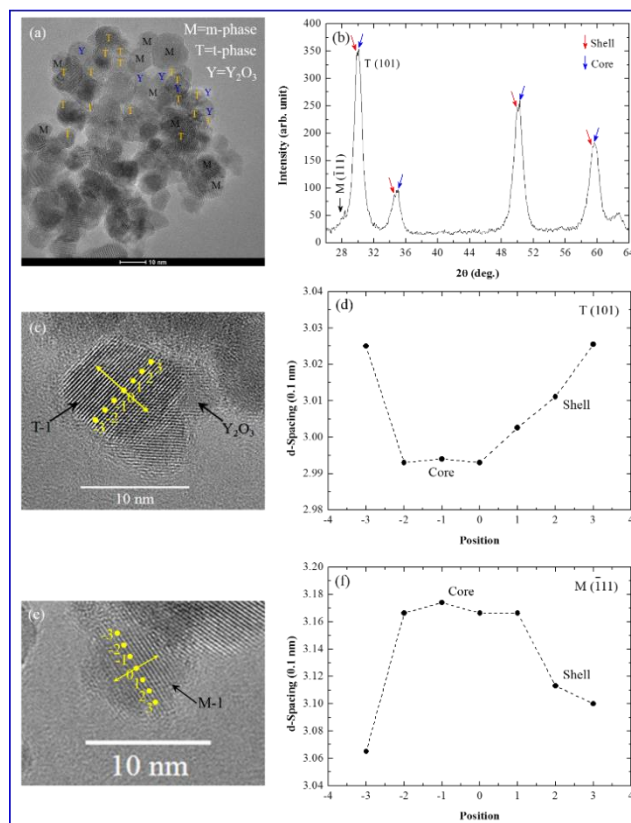
Fig. 5. Geometric phase analysis (GPA) of n-YSZ crystalline grain, the dashed circle shows the stress distribution.
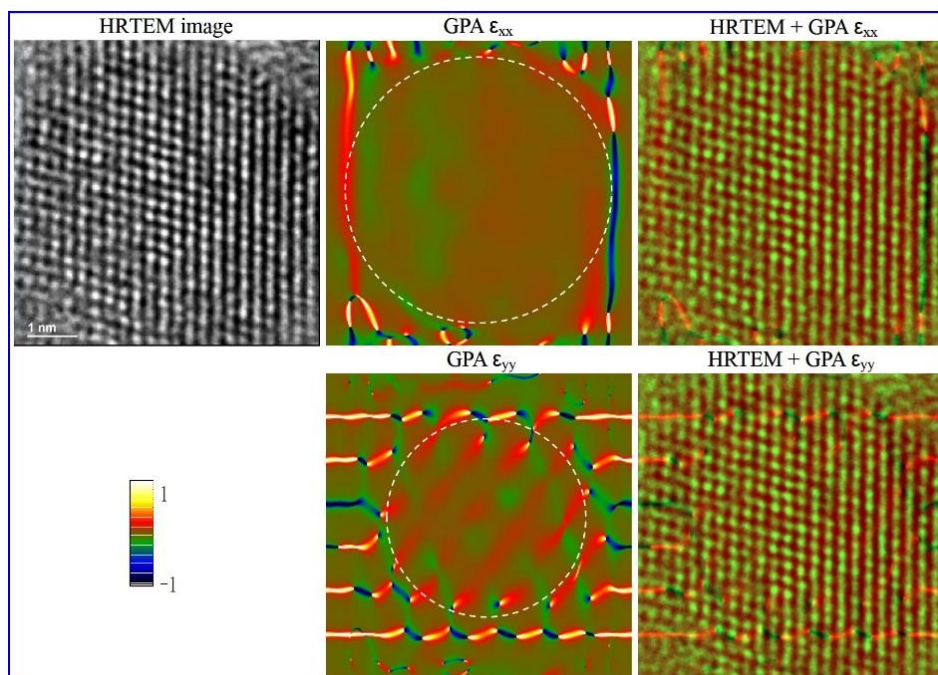
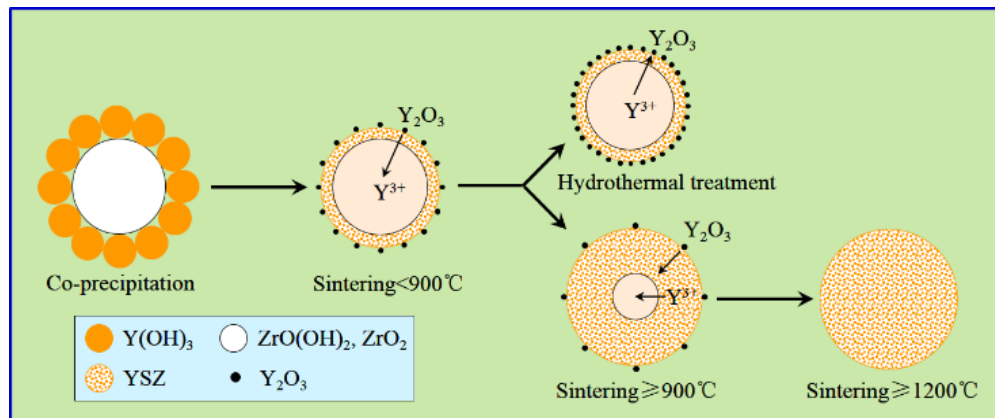**Fig. 6.** Effects of sintering and hydrothermal treatment on Y^{3+} diffusion, the center of the grain below 1200°C is YSZ with low content Y^{3+}.

Fig. 7. Residual Y_2O_3 (Curve 1) and M-phase (Curve 2) in powder P-18 after calcination at different temperatures between 600ºC and 1200ºC for 3 h (a) and at 1000ºC for 15 min up to 2 h (b). Crystalline grain sizes (Curve 1) of powder P-18 and thermal shock lives (Curve 2) of their corresponding coatings *vs* powder calcination temperature are compared in (c).
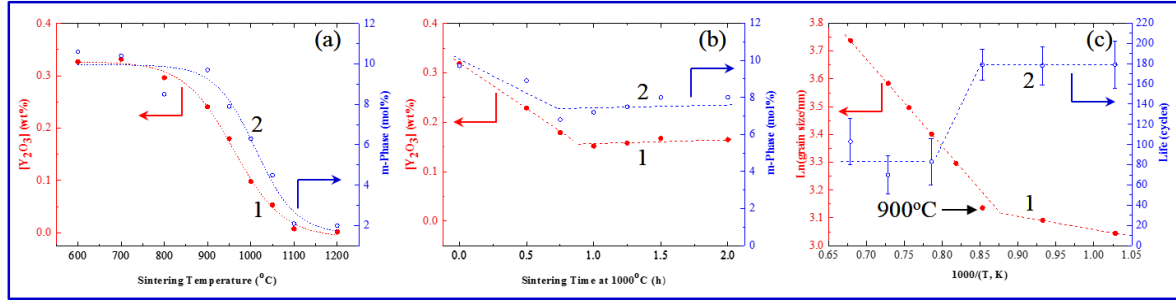
Fig. 8. SEM of n-YSZ coatings made by APS before (a~c) and after hydrothermal treatment for 10 days (d~f) in which cracking and corrosion of YSZ grains are obvious. Photograph (g) and SEM (h, i) of n-YSZ coatings after hydrothermal treatment for 40 days, semi- and unmelted particles, columnar and equiaxed grains are marked with A, B and C in (h, i), respectively. The corrosion of YSZ grains both on edges and surfaces are so serious that some grains are nearly spheroidized and corrosion pits in surfaces are obvious. Crystalline grain size (j), residual Y_2O_3 (Curve 1) and M-phase (Curve 2) contents in n-YSZ coatings after hydrothermal treatment for 3 h up to 40 days (k). XRD patterns of YSZ coatings after hydrothermal treatment for 3 h and 10 days are compared in (l). Both crystalline grain size and M-phase content are obtained from XRD measurements.
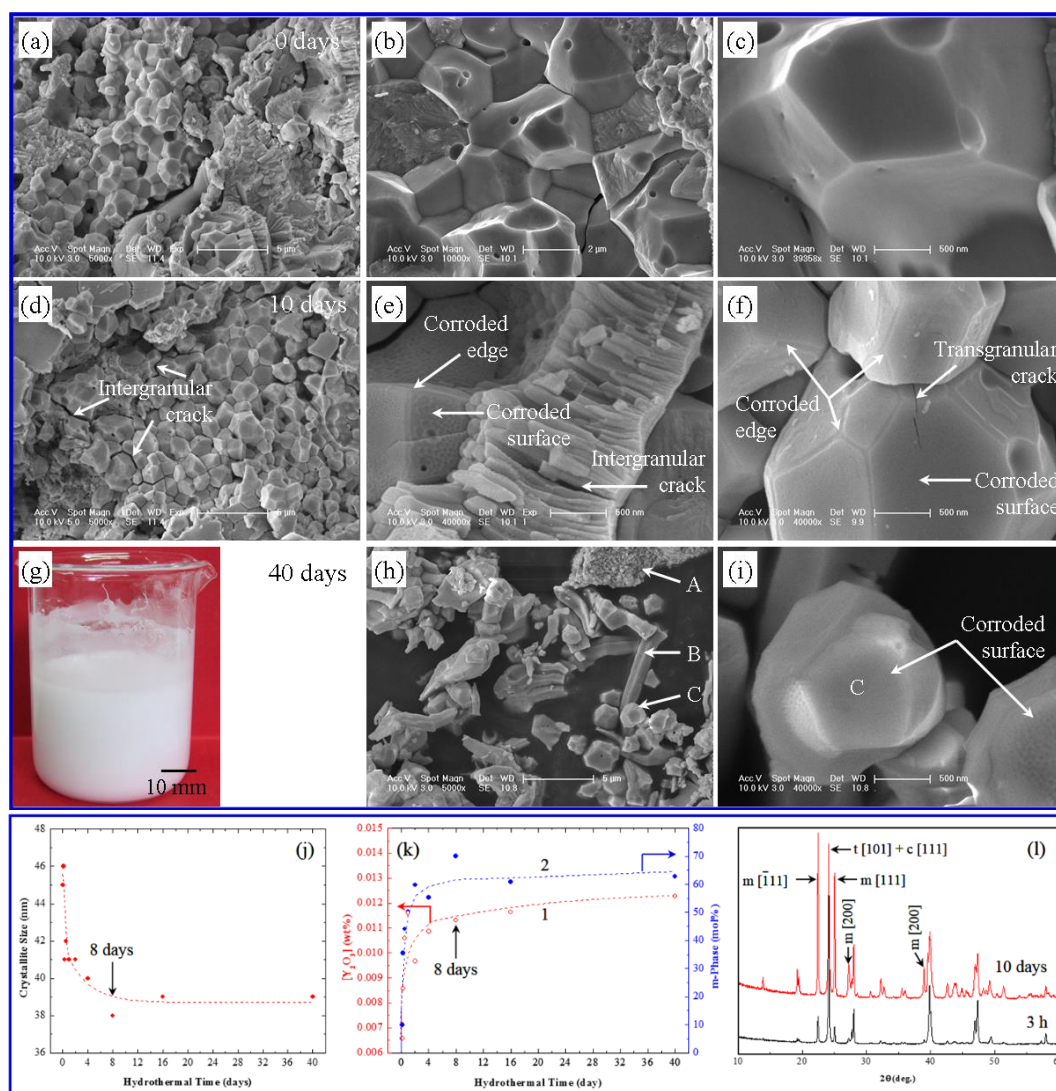
Fig. 9. (a) A small piece of 8YSZ target for EB-PVD which has been molten (T_m ~2800°C) by electron beam and cooled in vacuum, it looks shinning dark due to the formation of large quantity of oxygen vacancy; (b) The target was hydrothermally treated at 150°C for 10 days, the target was fully pulverized; (c) TGA of the target in air atmosphere: "Dark" is the sample in Fig. 9a, "Gray" is a sample which has not been molten by electron beam and looks gray.
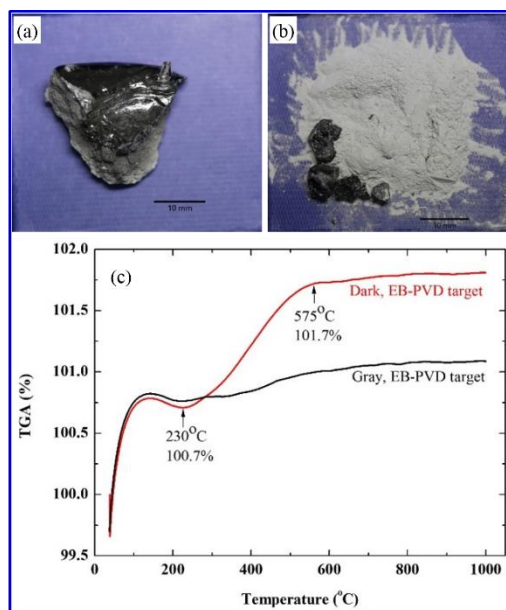
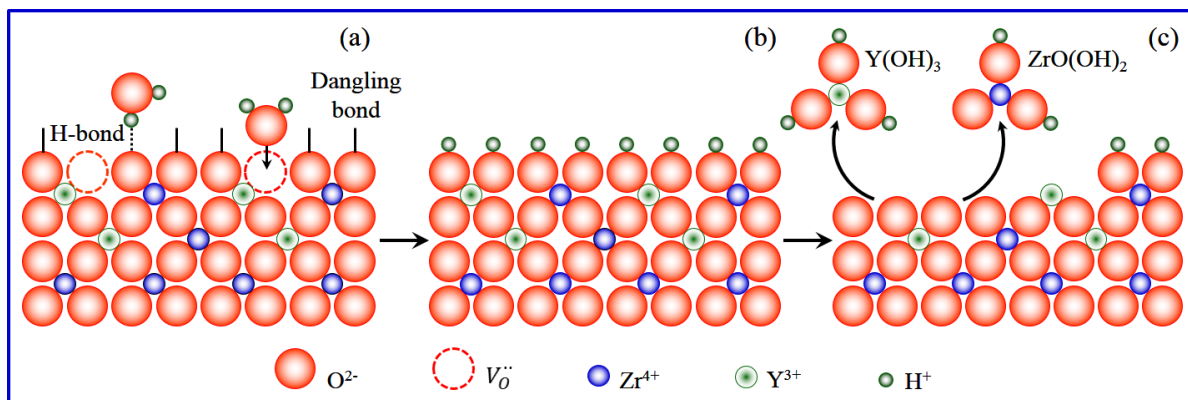**Fig. 10.** Schematic diagram for the hydrothermal corrosion process of YSZ.

Table 1 Contents of residual Y_2O_3 in YSZ powders.

Sample	YSZ Nanopowder	P-18	TZ-3Y	Zpex	YSZ	Green body for teeth	YSZ198U	NanoX S4007	YSZ
Source	Sigma Aldrich	Santong	Tosoh	Tosoh	CAAMS	Wieland	Inframat	Inframat	Xi An
Crystalline grain size (nm)	7	20	23	27	28	36	39	40	83
Total Y_2O_3 (wt%)*	13~14	7~8	5~6	5~6	7~8	5~6	7~8	7~8	7~8
Residual Y_2O_3 (wt%)	1.910	0.327	0.305	0.252	0.230	0.122	0.076	0.063	0.00287

*The total content of Y_2O_3 is obtained from the materials manual of its corresponding company.